Atherosclerosis 285 (2019) 55–63

Contents lists available at ScienceDirect

Atherosclerosis

journal homepage: www.elsevier.com/locate/atherosclerosis

^{18}F-FDG PET/MR-imaging in a Göttingen Minipig model of atherosclerosis: Correlations with histology and quantitative gene expression

Trine P. Ludvigsen[a], Sune F. Pedersen[b], Andreas Vegge[a], Rasmus S. Ripa[b], Helle H. Johannesen[b], Adam E. Hansen[b], Johan Löfgren[b], Camilla Schumacher-Petersen[c], Rikke K. Kirk[a], Henrik D. Pedersen[c,d], Berit Ø. Christoffersen[a], Mathilde Ørbæk[b], Julie L. Forman[e], Thomas L. Klausen[b], Lisbeth H. Olsen[c], Andreas Kjaer[b,*]

[a] Global Drug Discovery, Novo Nordisk Park, Novo Nordisk A/S, DK-2760, Måløv, Denmark
[b] Department of Clinical Physiology, Nuclear Medicine & PET and Cluster for Molecular Imaging, Dept. of Biomedical Sciences, Rigshospitalet and University of Copenhagen, Blegdamsvej 9, DK-2100, Copenhagen, Denmark
[c] Department of Veterinary and Animal Sciences, University of Copenhagen, Ridebanevej 9, DK-1870, Frederiksberg, Denmark
[d] Ellegaard Göttingen Minipigs A/S, Sorø Landevej 302, DK-4261, Dalmose, Denmark
[e] Section of Biostatistics, Department of Public Health, University of Copenhagen, Øster Farimagsgade 5, DK-1014, Copenhagen, Denmark

HIGHLIGHTS

- Diet-induced minipig model displays advanced human-like atherosclerosis.
- Correlation between *ex vivo* and *in vivo* assessment of plaque inflammation.
- Translational large animal model for targeting inflammation in atherosclerosis.

ABSTRACT

Background and aims: The advantage of combining molecular and morphological imaging, e.g. positron emission tomography and magnetic resonance imaging (PET/MRI), is reflected in the increased use of these modalities as surrogate endpoints in clinical trials. This study aimed at evaluating plaque inflammation using ^{18}F-fluorodeoxyglucose (^{18}F-FDG)-PET/MRI, and gene expression in a minipig model of atherosclerosis.

Methods: Göttingen Minipigs were fed for 60 weeks with fat/fructose/cholesterol-rich diet (FFC), chow (Control) or FFC-diet changed to chow midway (diet normalization group; DNO). In all groups, ^{18}F-FDG-PET/MRI of the abdominal aorta was assessed midway and at study-end. The aorta was analyzed using histology and gene expression.

Results: At study-end, FFC had significantly higher FDG-uptake compared to Control (target-to-background maximal uptake, TBR_{Max} (95% confidence interval) CI_{TBRMax}: 0.092; 7.32) and DNO showed significantly decreased uptake compared to FFC (CI_{TBRMax}: -5.94;-0.07). No difference was observed between DNO and Control (CI_{TBRMax}: −2.71; 4.11). FFC displayed increased atherosclerosis and gene expression of inflammatory markers, including vascular cell adhesion molecule 1 (*VCAM-1*), cluster of differentiation 68 (*CD68*), matrix metalloproteinase 9 (*MMP9*), cathepsin K (*CTSK*) and secreted phosphoprotein 1 (*SPP1*) compared to Control and DNO (all, $p < 0.05$). FDG-uptake correlated with gene expression of inflammatory markers, including *CD68*, $\rho_s = 0.58$; *MMP9*, $\rho_s = 0.46$; *SPP1*, $\rho_s = 0.44$ and *CTSK*, $\rho_s = 0.49$; ($p \leq 0.01$ for all).

Conclusions: In a model of atherosclerosis, ^{18}F-FDG-PET/MRI technology allows for detection of inflammation in atherosclerotic plaques, consistent with increased inflammatory gene expression. Our findings corroborate clinical data and are important in pre-clinical drug development targeting plaque inflammation.

1. Introduction

Cardiovascular disease is one of the greatest threats to global health with atherosclerosis as the main underlying cause [1]. An increased focus on plaque inflammation and stabilization has prompted exploration of biomarkers of inflammation in addition to morphological aspects of the disease [2] and with the advances in molecular and multimodal imaging, a novel era for visualization of disease has emerged,

* Corresponding author. Department of Clinical Physiology, Nuclear Medicine & PET and Cluster for Molecular Imaging, Rigshospitalet and University of Copenhagen, Denmark, Blegdamsvej 9, DK-2100, Copenhagen, Denmark.
E-mail address: akjaer@sund.ku.dk (A. Kjaer).

https://doi.org/10.1016/j.atherosclerosis.2019.04.209
Received 29 October 2018; Received in revised form 1 April 2019; Accepted 4 April 2019
Available online 09 April 2019
0021-9150/

focusing on functional disease aspects [3]. By use of positron emission tomography (PET) combined with either computerized tomography (PET/CT) or magnetic resonance imaging (PET/MRI), tracers targeting different stages of atherosclerosis have been exploited [3,4]. The radioactively labelled glucose analogue ^{18}F-fluorodeoxyglucose (^{18}F-FDG) has been validated in clinical settings and provides incremental predictive value to cardiovascular disease outcome, in addition to traditional risk markers [5]. The tracer correlates with findings of activated macrophages and markers of inflammation both at cellular-, protein- and RNA-level in human patients [6–8]. Also in relation to drug development, ^{18}F-FDG-PET has been emphasized as a relevant technology for assessing efficacy of cardiovascular drug candidates [9–11]. In the pre-clinical phase of drug development, it is a challenge to find optimal disease models of atherosclerosis [12–14]. Examples of misguided clinical trials as a consequence of erroneous extrapolation from pre-clinical studies, argues for optimization and a more critical approach to the pre-clinical drug development process [14]. The pig as a model for atherosclerosis, has several advantages compared to other existing models [15]; Firstly, the pathophysiology of the disease as well as the anatomical size of the arteries are comparable to human. Secondly, lesions progress to advanced plaques with morphological traits highly comparable to humans and the lesions reside in similar anatomical locations as in human patients [16,17]. Finally, the model allows application of clinical tools as used in humans [17] and the potential translational implications of this model of atherosclerosis in the context of drug development are compelling.

The aim of this study was to evaluate the feasibility of applying ^{18}F-FDG-PET/MRI in a Göttingen Minipig model of atherosclerosis to evaluate plaque inflammatory activity before and after change from an atherogenic to a standard minipig diet. Additionally, the aim was to evaluate correlations between plaque inflammation assessed *in vivo* and gene expression of plaque inflammatory markers assessed *ex vivo*.

2. Materials and methods

2.1. Animals and housing

Castrated male Göttingen Minipigs (*Sus scrofa*), mean age 28 weeks (standard deviation (SD) ± 1 week) at study start, were housed at the experimental animal unit facilities of University of Copenhagen, Denmark. Animals were kept in a natural day/night cycle, in a relative humidity of 50–70%, at controlled room temperature, with free access to water and bedding material, according to existing regulations. The animals were a part of a larger study and data regarding other research topics have been included in other publications [18,19]. The study was approved by the Animal Experiment Inspectorate, Ministry of Justice, DK.

2.2. Study design

The total study duration was 56–60 weeks, with animals evaluated midway (mid-study) and at study-end (end-study). Three groups of animals were included in the study: (1) Lean control animals (Control, n = 3), fed standard chow (Mini-Pig Expanded, Special Diets Services, Witham, UK) during the entire study, (2) a group fed fat/fructose/cholesterol diet (FFC, n = 6)(Test diet®, Missouri, USA) for the entire study duration and (3) a group fed fat/fructose/cholesterol diet until mid-study, followed by diet normalization to standard chow until end-study assessments (DNO, n = 8). A staggered study design was applied, with all groups represented in three cohorts, with 5–7 week interval between cohorts. The study design is further described in Supplementary appendix 1.

2.3. Plasma analysis

Blood samples were collected 4–7 weeks prior to *in vivo* imaging. Measurements of total cholesterol in plasma were performed on Cobas®6000 autoanalyzer (Roche Diagnostics A/S, Hvidovre, DK) according to the guidelines of the manufacturer. Measurements of C-reactive protein (CRP) in serum were performed as previously described, using a dendrimer-coupled cytidine diphosphocholine sandwich immunosorbent enzymebound assay (ELISA) [16,20].

2.4. Animal preparation, anesthesia and analgesia protocol

Overnight fasted animals were anesthetized using repeated IM injections of a zolazepam and tiletamin mixture (Zoletil 50 Vet., ChemVet, Silkeborg, DK) with added ketamine, xylazine and butorphanol as previously described [21]. IV access was established in either the auricular or the saphenous vein and the animals were intubated, but kept at spontaneous respiration with supplied oxygen. Additionally, a percutaneous suprapubic catheter was implanted to allow bladder emptying during the entire procedure. Vital parameters were monitored objectively by pulsoximetry and subjectively by a qualified research veterinarian. Immediately prior to tracer-injection, blood glucose was measured to ensure glucose ≤7 mmol/L (≤126 mg/dl). ^{18}F-FDG was injected intravenously at activity levels of 365–426 MBq (mean 402 MBq), 3 h before PET acquisition, as previously described [22]. See Supplementary appendix 1 for further details.

2.4.1. MRI and PET acquisition

Simultaneous PET/MRI was performed using a Biograph mMR (Siemens Healthcare, Erlangen, Germany), with one spine and two body surface receive coils positioned at the abdomen and thorax. A T1 Turbo Spin Echo (TSE) served to center a PET acquisition [1 bed position, post injection delay 180 min, 10 min acquisition time] on the point of the abdominal aorta midway between the iliac trifurcation and renal arteries. During the PET acquisition, a DIXON sequence [repetition time (TR)/echo time (TE) = 3.6/1.23 ms and 2.46, flip angle 10°, Field-of-View (FOV) 500 mm, 128 slices, slice thickness/gap 3.1/0.0 mm, pixel size 4.1 × 2.6 mm^2] and a transverse T2 Half-Fourier-Acquired Single-shot Turbo spin Echo (HASTE) [TR/TE = 3000/87 ms, flip angle 160°, FOV 380 mm, 33 slices, slice thickness/gap 5.0/1.0 mm, pixel size 1.5 × 1.2 mm^2] was acquired. Additionally, both during and after the PET, a 3D T2 weighted Sampling Perfection with Application optimized Contrasts using different flip angle Evolution (SPACE) sequence [TR/TE = 1500/111 ms, FOV 401 mm, 112 slices, slice thickness/gap 1.2/0.0 mm, pixel size 0.6 × 0.6 mm^2] and transverse T1 water saturated TSE [TR/TE = 685/9.5 ms, flip angle 140°, FOV 500 mm, 27 slices, slice thickness/gap 6.0/1.2 mm, pixel size 1.8 × 1.3 mm^2] was obtained.

2.4.2. PET reconstruction

The PET data were reconstructed using ordered-subsets expectation maximization iterative reconstruction algorithm (OSEM 3D) [3 iterations, 21 subsets, 2 mm post filtering 3D Gauss, matrix 344 × 344, voxel size 2.1 × 2.1 × 2.0 mm^3] with MRI-based attenuation correction derived from the DIXON sequence [23].

2.4.3. Image analysis – PET quantification

Guided by MRI, regions of interest (ROI) were drawn free-hand on transaxial image slices covering vessel and lumen of the entire abdominal aorta. ROIs were then superimposed onto the PET data whereby mean and maximum standardized uptake values (SUV_{Mean}, SUV_{Max}) of ^{18}F-FDG-tracer concentration were obtained reporting an average value of all evaluated segments. To obtain target-to-background ratios (TBR), mean tracer concentration was obtained from ROIs in the abdominal paraspinalis muscles correcting for basal tissue activity ($SUV_{Mean/Max}/SUV_{Paraspinalis}$ = TBR) yielding TBR_{Mean} and TBR_{Max}.

Further details on image analysis are given in Supplementary appendix 1.

Table 1
In vivo parameters group differences over time.

	Mid-study			End-study		
	Control (n = 3)	FFC (n = 6)[a]	DNO (n = 8)[a]	Control (n = 3)	FFC (n = 5)	DNO (n = 7)
BW (kg)	29 ± 1^{A}	41 ± 6^{B}	40 ± 2^{B}	38 ± 1^{B}	75 ± 14^{C}	51 ± 3^{D}
TC (mM)	2.3 ± 0.5^{A}	23.2 ± 8.8^{B}	17.6 ± 7.3^{BC}	1.9 ± 0.5^{A}	14.3 ± 2.8^{C}	1.9 ± 0.5^{A}
TBR_{Mean}	2.4 ± 0.7	3.4 ± 1.3	3.5 ± 2.2	2.4 ± 0.4	3.7 ± 1.6	2.8 ± 0.8
TBR_{Max}	3.7 ± 1.9^{A}	5.9 ± 2.5^{A}	6.0 ± 3.9^{A}	3.7 ± 1^{A}	7.0 ± 3.7^{B}	4.7 ± 1.2^{A}
SUV_{Mean}	0.43 ± 0.04	0.49 ± 0.23	0.54 ± 0.27	0.48 ± 0.09	0.68 ± 0.2	0.53 ± 0.24
SUV_{Max}	0.67 ± 0.03^{A}	0.87 ± 0.45^{A}	0.93 ± 0.45^{A}	0.75 ± 0.17^{A}	1.38 ± 0.48^{B}	0.88 ± 0.35^{A}

Group data are displayed as mean ± SD. Different uppercase letters indicate statistically significant difference between groups ($p < 0.05$).
Control: lean control group; FFC: fat/fructose/cholesterol-fed group; DNO: diet normalization group; BW: body weight; TC: total cholesterol; $TBR_{Mean\ or\ Max}$: mean or maximum target-to-background uptake, $SUV_{Mean\ or\ Max}$: standardized uptake value, mean or maximum uptake.
[a] For the tracer uptake, only n = 5.

2.5. Tissue harvesting

The animals were euthanized in surgical anesthesia (described above) by exsanguination. The aorta was sampled *in toto* and three transverse slices of approximately 6 mm thickness were harvested from the abdominal aorta: one section immediately caudal to the most caudally located renal artery, one cranially to the aortic trifurcature and one final slice centered between the two. Each slice was split in two and one was snap frozen in liquid nitrogen and transferred to −80 °C storage for later RNA extraction and one was immersion-fixated in 10% neutral-buffered formalin (NBF) for 24 h before processing and paraffin embedding. The remaining parts of the aorta were opened ventrally at the long axis, fixed on a Styrofoam plate and immersion-fixed in 10% NBF for a minimum of 24 h.

2.5.1. Ex vivo assessment of the aorta

2.5.1.1. Histology. Histological assessments included plaque burden (intima-media thickness (IMT)), reporting average values from the three segments and plaque morphology from standard histochemically-stained segments. Additionally, morphometry of immunohistochemical stainings for CD68 $^{+}$ and α-smooth muscle actin+ (α-SMA) cells was performed to quantify plaque inflammation. For qualitative assessments, lesion morphology in the aorta was classified according to modified human guidelines and previous findings in minipigs [16,24,25], distinguishing between non-pathological intimal lesions and pathological intimal thickening, the latter including fibroatheroma and thin-capped fibroatheroma, with the most advanced finding per animal reported.

2.5.1.2. En face. Aortic plaque burden was measured *en face* as the percentage ratio of macroscopic lipophilic stained aortic area (Sudan IV, Alfa Aesar, Karlsruhe, GE) in the total aortic area, using image analysis software (VIS™, Visiopharm, Hørsholm, DK), as previously described [16].

2.5.1.3. Tissue RNA extraction and cDNA synthesis. Tissue conservation and cDNA synthesis for real-time qPCR analysis was modified from clinical procedures as previously described [8,26,27], and by use of the AffinityScript™ qPCR cDNA Synthesis Kit (Agilent Technologies Inc., Santa Clara, CA, USA), 1 ng of total RNA was subsequently reverse transcribed to cDNA for subsequent real-time qPCR analysis of whole-slice gene expression.

2.5.1.4. Quantitative real-time PCR. TaqMan® based gene expression assays were designed using Beacon Designer™ 8.14 (PREMIER Biosoft, Palo Alto, CA, USA) and analyzed using Mx3000P® or Mx3005P™ real-time PCR systems (Stratagene, La Jolla, CA, USA). Eight genes of interest were selected; cluster of differentiation 68 (*CD68*, gene ID: NM_001291776), cluster of differentiation 163 (*CD163*, gene ID: NM_213976), chemokine (C−C motif) ligand 2 (*CCL2*, gene ID: NM_214214), cathepsin K (*CTSK*, gene ID: NM_214302), matrix metalloproteinase 9 (*MMP9*, gene ID: NM_001038004), myosin heavy chain 11 (*MYH11*, gene ID: XM_013991919), secreted phosphoprotein 1 (*SPP1*, gene ID: NM_214023), vascular cell adhesion molecule 1 (*VCAM-1*, gene ID: NM_213891). Selection of housekeeping genes was based on previous work in pigs [28].

For further details on *ex vivo* assessments, please consult Supplementary appendix 1.

2.6. Statistical analysis

Data are summarized as mean and SD unless otherwise stated. For evaluation of changes over time and differences between groups, a linear mixed model was applied with cohort, time, and group as fixed effects and animal ID as random effect. Differences between gene expression levels across groups were evaluated in a similar model, with animal ID as a random effect to account for replicate segments from each animal. Normality of the data was evaluated in a residual plot and data transformed if required. Spearman's rank correlation was computed between tracer uptake (TBR_{Max}, TBR_{Mean}; SUV_{Max} and SUV_{Mean}) and gene expressions and assessed by use of a permutation test, accounting for replicate segments from each animal. 95% confidence intervals and *p*-values were reported.

All statistical analyses were performed using relevant software, either SAS® version 9.2, (Cary, North Carolina, USA) or for the permutation test, R version 3.4.2 [29]. Graphical presentations were performed in GraphPad Prism® version 6.07 (La Jolla, California, USA).

3. Results

Of 17 included animals, n = 13 were scanned mid-study and n = 15 were scanned end-study, with a total of 11 animals completing both scans.

3.1. In vivo assessment of atherosclerosis: ^{18}F-FDG PET/MRI

In Table 1, an overview of the results of TBR and SUV from both scans is displayed. Figs. 1 and 2 illustrates representative MRI, ^{18}F-FDG PET/MRI and ^{18}F-FDG PET images mid- and end-study and Fig. 3 illustrates the difference in TBR and SUV values between mid- and end-study assessments. When evaluating FDG-uptake end-study (see Table 1), FFC animals had significantly increased TBR_{Max} compared to Control (95% confidence interval, (CI_{TBRMax}: 0.09; 7.32, $p = 0.045$), and DNO showed a significantly decreased uptake compared to FFC (CI_{TBRMax}: −5.94;-0.07, $p = 0.046$), whereas no difference was observed between Control and DNO (CI_{TBRMax}: −2.71; 4.11, $p = 0.66$). The same trend was observed for TBR_{Mean} in the group comparisons, although not reaching statistical significance ($CI_{FFC\ vs.\ Control}$: −0.15;

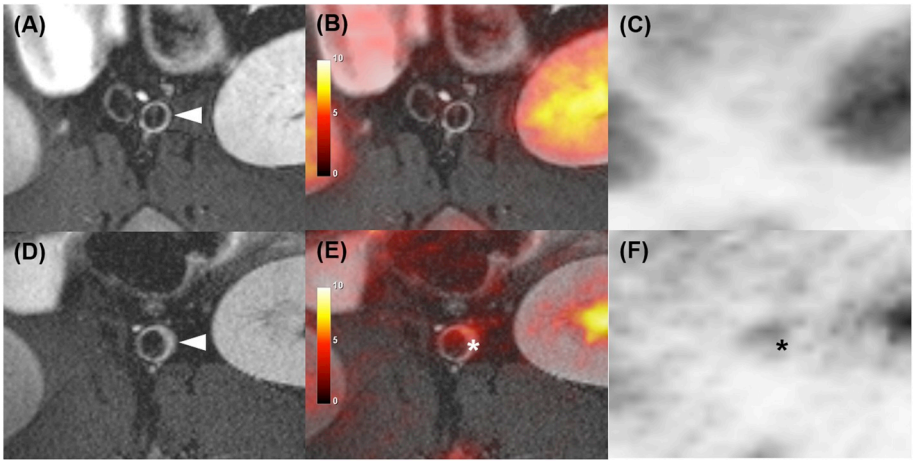

Fig. 1. *In vivo* transaxial PET/MRI findings in the abdominal aorta of fat/fructose/cholesterol fed (FFC) animal.
Mid-study images (A–C), end-study images (D–F). T2-weighted MR images (A and D), combined PET/MRI (B and E) and PET (C and F). Left pointing arrows depict abdominal aorta (A and D), asterisks depict abdominal aorta plaque and enhanced ^{18}F-FDG-uptake (E and F).

3.24, $p = 0.07$, $CI_{DNO\ vs.\ FFC}$: −2.62; 0.12 $p = 0.07$, $CI_{Control\ vs.\ DNO}$: −1.30; 1.9, $p = 0.68$)). Overall data indicates increased glycolytic activity in the FFC group compared to DNO and control animals. Findings were comparable for the SUV values. As shown in Fig. 3, difference between FDG-uptake from mid-to end-study assessments did not reach statistical significance across the groups.

CRP levels were not different between groups or times and displayed large degree of variation. Data is presented in Supplementary appendix 2.

3.2. Ex vivo assessment of atherosclerosis: en face, immunohistochemistry, histology and gene expression

Data from *ex vivo* assessments is displayed in Tables 2 and 3. Significant differences between groups in aortic *en face* plaque area as well as plaque burden (IMT) were observed for FFC compared to Control ($CI_{En\ Face}$: 2.17; 7.63, $p = 0.002$ and CI_{IMT}: 1.13; 3.58, $p = 0.001$), as well as for DNO compared to Control ($CI_{En\ Face}$: 0.34; 5.49, $p = 0.03$ and CI_{IMT}: 0.38; 2.77, $p = 0.013$). No difference between DNO and FFC was observed for *en face* plaque area ($CI_{En\ Face}$: −4.22; 0.24, $p = 0.08$) or IMT (CI_{IMT}: −1.84; 0.28, $p = 0.16$). Content of α-SMA normalized to intima area was no different between DNO and FFC ($CI_{\alpha\text{-}SMA}$: 0.12; 0.02, $p = 0.14$), nor was CD68 normalized to intima area CI_{CD68}: −0.0007; 0.007, $p = 0.11$). Fig. 4 depicts examples of aorta *en face* from representative animals of each group. For plaque morphology, representative examples of findings are illustrated in Fig. 5. In summary, advanced plaque findings ranged from normal or non-pathological intimal thickening (Control, n = 3 and DNO, n = 2) to pathological intimal thickening (FFC, n = 2 and DNO, n = 5), to fibroatheroma (FFC, n = 3).

For gene expression, a total of 45 slices from 15 animals were recovered. As shown in Table 3, FFC displayed an overall more inflammatory plaque phenotype compared to Control and DNO, in line with the *in vivo* PET-data. Specifically, significantly increased expression of *VCAM-1*, *CD68* and the plaque remodeling markers (*MMP9*, *CTSK* and *SPP1*) was observed in FFC compared to DNO and Control. In DNO, expression levels of *CD68* and *CTSK* were comparable to Control, whereas *MMP9*, and *SPP1* were increased. The difference in expression in *MYH11* was inverse to that of the inflammatory markers given above with the FFC being significantly reduced compared DNO and Control. With regards to *CD163* no significant group differences were observed.

3.3. Ex vivo and in vivo correlations: gene expression and ^{18}FDG-uptake

FDG-uptake (TBR_{Mean} and TBR_{Max}) correlated positively with genes for plaque inflammation and remodeling, *CD163* (TBR_{Mean}: $\rho_S = 0.51$, $p = 0.002$; TBR_{Max}: $\rho_S = 0.41$, $p = 0.024$), *CD68* (TBR_{Mean}: $\rho_S = 0.46$, $p = 0.003$; TBR_{Max}: $\rho_S = 0.58$, $p = 0.0005$), *CTSK* (TBR_{Mean}: $\rho_S = 0.41$, $p = 0.005$; TBR_{Max}: $\rho_S = 0.49$, $p = 0.002$), *MMP9* (TBR_{Mean}: $\rho_S = 0.43$, $p = 0.018$; TBR_{Max}: $\rho_S = 0.46$, $p = 0.009$) and *SPP1* (TBR_{Mean}: $\rho_S = 0.34$, $p = 0.026$; TBR_{Max}: $\rho_S = 0.44$, $p = 0.011$). Fig. 6 depicts correlations and group distributions between TBR_{Max} and gene expression. Similar correlations were observed for $SUV_{Max/Mean}$ and are presented in Supplementary appendix 2, in addition to other results.

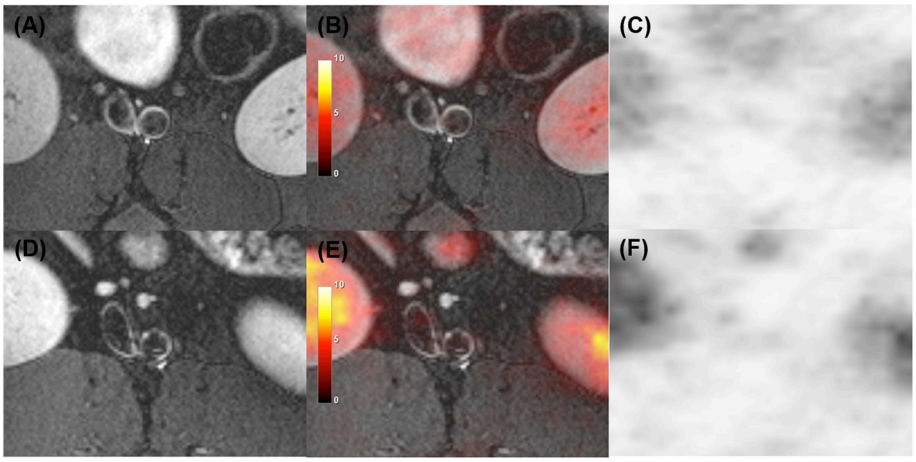

Fig. 2. *In vivo* transaxial PET/MRI findings in the abdominal aorta of diet normalization animal (DNO).
Mid-study images (A–C), end-study images (D–F). T2-weighted MR images (A and D), combined PET/MRI (B and E) and PET (C and F).

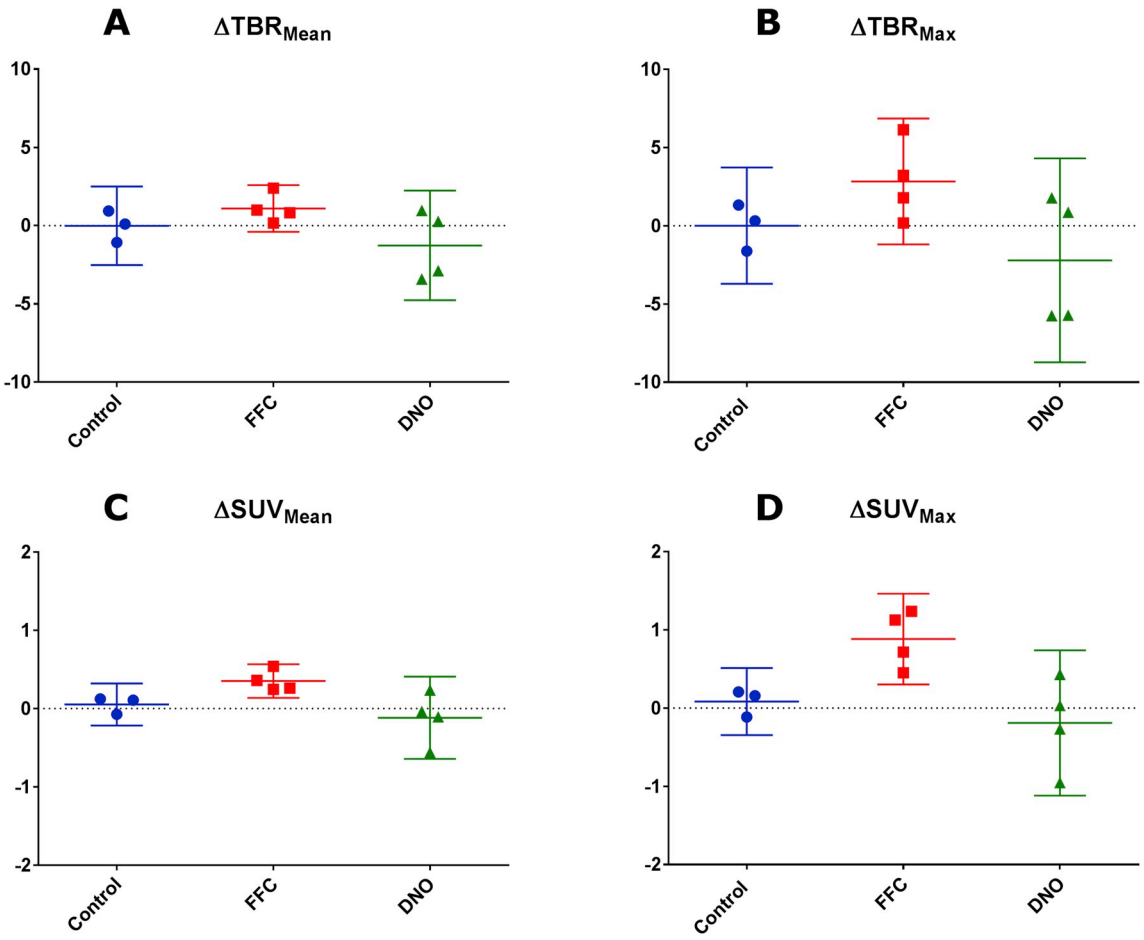

Fig. 3. Illustration of distribution in paired tracer uptake from mid-to end-study assessments in the animals that completed both assessments.
No significant differences were observed from paired evaluations. Mean and confidence interval (95%) is displayed. $TBR_{Mean\ and\ Max}$: mean or maximal target to background ratio. Control: lean control group; FFC: fat/fructose/cholesterol-fed group; DNO: diet normalization group.

Table 2
Ex vivo group differences.

	Control (n = 3)	FFC (n = 5)	DNO (n = 7)
En face plaque area[a] (%)	0.4^{A} (0.3–0.6)	80.8^{B} (36–85.3)	10.5^{B} (1.1–44.6)
IMT[a] (μm^2)	0.02^{A} (0.02–0.04)	0.29^{B} (0.20–0.36)	0.14^{B} (0.12–0.14)
CD68 area (μm^2)	n/a	0.005 ± 0.003	0.002 ± 0.002
α-SMA (μm^2)	n/a	0.16 ± 0.03	0.22 ± 0.05

Group data are displayed as mean ± SD. Different uppercase letters indicate significant difference ($p < 0.05$).
Control: lean control group; FFC: fat/fructose/cholesterol-fed group; DNO: diet normalization group; *En face*: plaque burden evaluated *en face* in aorta; IMT: intima-media thickness; CD68: $CD68^{+}$ cells corrected for intimal area; α-SMA: smooth muscle cell ratio corrected for intimal area.
[a] Data log-transformed for normality and presented as median and interquartile range.

Table 3
Fold change in gene expression.

	Fold change		
Name	Control (n = 3)	FFC (n = 5)	DNO (n = 7)
CCL2	4.1 ± 2.8	8.8 ± 6.8	5.3 ± 4.7
CD163	3.9 ± 3.0	12.2 ± 12.4	4.1 ± 3.2
CD68	5.3 ± 3.4^{A}	49.5 ± 33.4^{B}	16.7 ± 17.5^{A}
CTSK	3.4 ± 2.0^{A}	4.5 ± 3.1^{B}	4.4 ± 3.5^{A}
MMP9[a]	5.56^{A} (3.72–8.23)	452.64^{B} (134.26–924.30)	62.63^{C} (8.39–303.81)
MYH11	30.1 ± 17.7^{A}	9.9 ± 10.3^{B}	23.0 ± 14.9^{A}
SPP1	4.4 ± 2.3^{A}	933 ± 824^{B}	108.2 ± 201.7^{C}
VCAM-1	2.8 ± 1.3^{A}	9.8 ± 5.0^{B}	2.8 ± 1.7^{A}

Data is shown as mean ± SD. Different uppercase letters indicate significant difference ($p < 0.05$).
Control: lean control group; FFC: fat/fructose/cholesterol-fed group; DNO: diet normalization group; CCL2: chemokine (C−C motif) ligand 2; CD: Cluster of differentiation; CTSK: cathepsin K; MMP9: matrix metalloproteinase 9; MYH11: smooth muscle myosin heavy chain; SPP1: secreted phosphoprotein 1; VCAM-1: vascular cell adhesion molecule 1.
[a] Data is log-transformed for normality.

4. Discussion

In this study, a Göttingen Minipig model of human atherosclerosis was evaluated, using repeated in vivo assessment by ^{18}F-FDG-PET/MRI before and after change from an atherogenic to a healthy diet. Histologically, the advanced atherosclerotic lesions were morphologically comparable to human findings, with dietary normalization overall ameliorating plaque inflammation. The *in vivo* assessments by PET showed increased vascular inflammation following long-term atherogenic diet feeding as compared to chow-fed animals. In addition, cessation of the atherogenic diet resulted in reduction of the vascular inflammation after approximately 6 months. Overall, tracer uptake correlated well with gene expression of plaque inflammation. The present observations correspond to clinical findings in human atherosclerosis, supporting the translational potential of the model.

The current study design was based on a previous study with advanced atherosclerotic lesions reported after 22 weeks of dietary intervention in Göttingen Minipigs [16]. In previous regression studies in

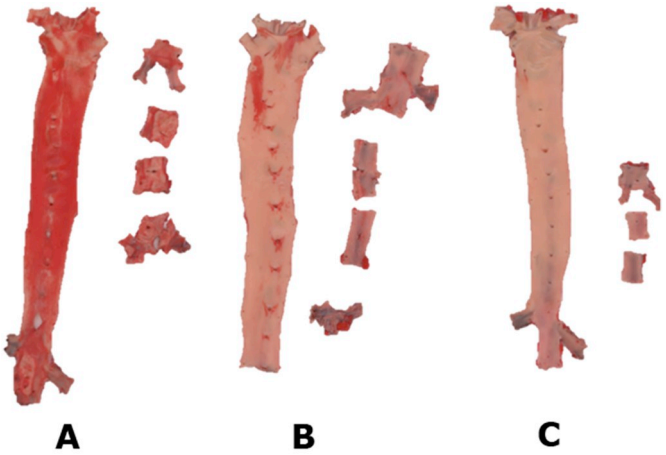

Fig. 4. Examples of aorta *en face,* stained with Sudan IV, abdominal aorta is segmented due to sampling for histology.
(A) Fat/fructose/cholesterol-fed animal, (B) diet normalization animal, (C) lean control animal.

pigs, effects on morphological traits including intra-plaque hemorrhage and necrotic core reduction has been observed after 14 treatment months [30], whereas decrease in intimal proliferative activity was observed already after 4.5 months [31]. Using PET-technology in clinical studies, intervention effect on plaque inflammation has been reported after minimum 3 months of treatment [12,32], and duration of intervention in the current study was expected to result in an effect of FFC diet cessation on plaque composition. Although not statistically significant over time, our findings are consistent with the observations in humans, that an effect on plaque inflammation is observed within a relatively short period of intervention, and that this effect can be detected by *in vivo* FDG-PET-imaging [32]. In the current study, we evaluated the global FDG-uptake in the abdominal aorta, and accordingly sampled tissue from pre-defined locations in the aorta. A different approach could have been to evaluate intervention effect on most-diseased segment as previously reported [32,33].

Significant correlations between *ex vivo* molecular markers of plaque inflammation and *in vivo* tracer uptake were observed, consistent with what has been shown from endarterectomy specimens from human patients [8,34]. The porcine aortic expression of the scavenger receptor (*CD68*) correlated well with FDG-uptake as well as immunohistochemical staining of CD68-positive cells ($R^2 = 0.59$, $p = 0.0008$; data not shown). An important note is that CD68 is not unique to macrophages and evidence suggest that 30% or more of CD68-expressing cells in advanced coronary atherosclerosis have a non-myeloid origin (e.g. vascular smooth muscle cells) [35]. Notwithstanding, CD68 expression in atherosclerosis is considered a measure of macrophage load and is associated with the severity of carotid plaque inflammation [36]. Hemoglobin scavenger receptor CD163 is expressed by hemorrhage-associated macrophages and proposed as an unique M2 subtype suggestively identified as M(Hb), that exert an atheroprotective role [37]. However, some controversy exists in this regard [38]. In our study, although CD163 correlated with FDG-uptake, no group differences were observed in gene expression levels. Additionally, SPP1, known as osteopontin, also correlated with tracer uptake, which is consistent with osteopontin being associated with the inflammatory milieu of the plaque [39].

In the DNO group, the inflammatory gene expression levels were overall closer to that of the control animals, although the expression of plaque remodeling markers MMP9 and CTSK were intermediate between Control and FFC. The latter indicate a reduced plaque matrix remodeling activity in DNO compared to FFC. In our study the MYH11 marker was selected in order to specifically target the contractile vascular smooth muscle cell [40,41]. MYH11 gene expression did not correlate with FDG-uptake and it was expressed in comparable levels between Control and DNO, with decreased levels in FFC compared to Control and DNO, although statistical significance was not reached. However, a decrease could indicate de-differentiation of vascular smooth muscle cells from a contractile to a synthetic phenotype associated with atherogenesis. These findings, in conjunction with reduced inflammatory marker expression in the DNO, indicate a shift from a more inflamed plaque to a more stable plaque phenotype as a result of atherogenic diet-cessation. Of interest, plaque burden (IMT and *en face*) only tended to be decreased in DNO compared to FFC and DNO, whereas differences were detectable at gene expression levels, confirming that plaque activity is much more dynamic than plaque burden, in line with clinical findings [42,43].

The selection of ^{18}F-FDG as tracer relies on the established use in patients as well as its availability combined with a well-described safety profile. Although ^{18}F-FDG may not be macrophage specific, it is a standard tracer, available across research sites, and until now the most investigated tracer within the field of atherosclerosis. Interestingly, in atheroma formation, hypoxia locally in the plaque, has been associated with altered glucose metabolism, as depicted by increased ^{18}F-FDG-uptake in lesions [44]. The glucose uptake in the vessel signified by ^{18}F-FDG signal intensity thus reflects a complex interplay between pro-inflammatory stimuli and a local hypoxia [7].

In the current study, the arterial segment targeted was the abdominal aorta. In patients, aortic atherosclerosis correlate with a previous history of unstable angina pectoris [45], supporting the relevance of the aorta as surrogate marker of coronary atherosclerosis in human patients. In previous minipig studies, more advanced lesions were

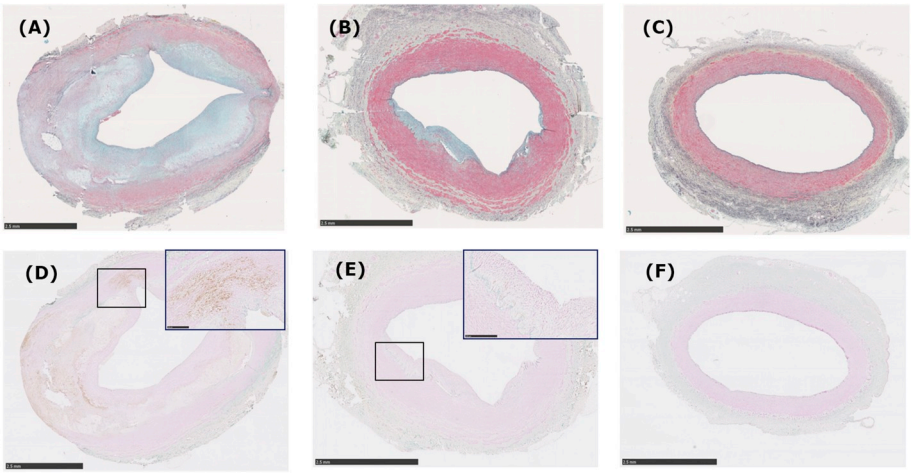

Fig. 5. Examples of plaque findings in abdominal aortas across groups.
Fat/fructose/cholesterol fed animal (A and D), diet normalization animal (B and E) and lean control (C and F). Upper panel (A–C) Movat's pentachrome staining, lower panel triple staining of cluster of differentiation 68 (CD68), α-smooth muscle cell actin and elastic membrane (D–F). Inserts in D and E, show CD68 $^{+}$ areas. However, difference between CD68 $^{+}$ in DNO and FFC did not reach statistical significance.

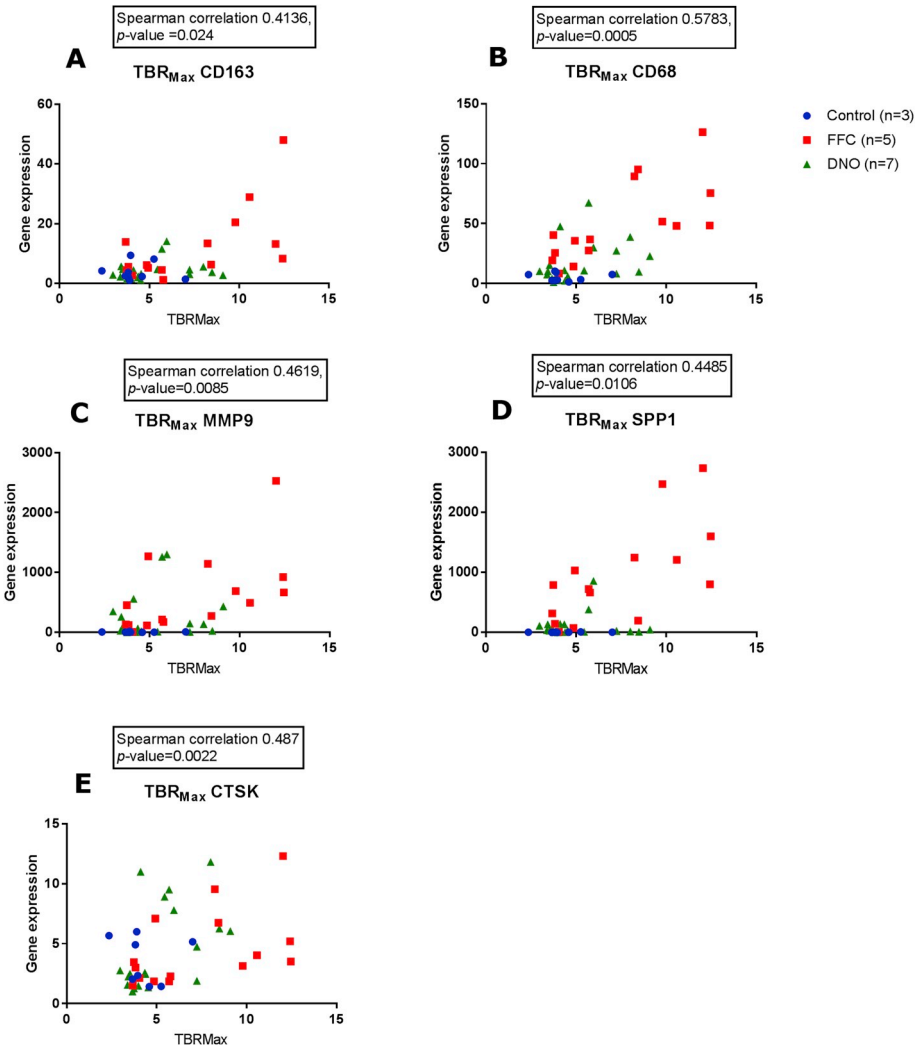

Fig. 6. Correlations between tracer uptake (TBR_{Max}) and gene expression levels of *CD163* (A), *CD68* (B), *MMP9* (C), *SPP1* (D) and *CTSK* (E).
From each individual, 2–3 segments are displayed. Spearman correlations with adjusted p-values based on a permutation test. A $p < 0.05$ is considered significant. TBR_{Max}: Maximal target-to-background ratio, FFC: fat/fructose/cholesterol group, DNO: diet normalization group, Control: lean control group, CD: cluster of differentiation. MMP: matrix metalloproteinase, SPP1: secreted phosphoprotein 1, CTSK: cathepsin K.

observed in the aorta, compared to coronary arteries [16,46,47] and also in humans, some heterogeneity in the distribution of atherosclerosis between vascular beds has been observed [48], but with a strong association in degree of FDG-uptake across various vascular beds [49]. An important limitation in the study in general, is the number of animals included in the study, in particular considering normal group sizes required when evaluating intervention effects in pre-clinical models. Using a clinical scanner as in the current study is both costly and logistically complex and thereby limited the number of animals that we included in our study. The resulting lack of power is a limitation for the conclusions that can be derived from the study. However, the study provides valuable information for future power calculations in a similar set-up. Missing data were handled by the application of linear mixed models in the statistical analyses, which provide optimal and unbiased inference under the assumption that missing data are missing at random. If this assumption fails, results may be biased. Different from human assessments, the animals needed to be anesthetized for the procedures with a potential influence on hemodynamics and/or plasma glucose levels, although the latter was monitored. With regards to *in vivo* plaque morphology, the MRI applications used in the current study did not allow for these assessments, and merely served as anatomical guidance for registration of tracer signal. For the purpose of the current study, the PET/CT technology could be an alternative, with the perspective of a shorter scan time. CT also provides an opportunity for a non-invasive assessment of inflammation related to the coronary vessels [50], using the perivascular fat attenuation index [50]. In the paper by Oikonomou et al., the method was shown to enhance prediction of cardiac risk factors, beyond what CT angiography could provide. This method could be an interesting perspective in a pre-clinical model to capture an indirect marker of coronary artery inflammation. Previous studies in humans have shown capability of detailed assessment of both plaque burden as well as composition using MRI, however, the position of the arteries were more superficial (e.g. carotid arteries) compared to the abdominal aorta assessed here. The carotid arteries in pigs are, however, not anatomically comparable to human, and therefore not relevant for assessments.

The comparability of SUV to TBR in this study confirms that SUV represents a valid marker for FDG-uptake in the vessel wall when images are acquired 3 h after FDG injection.

In summary, the ^{18}F-FDG-PET/MRI technology detected molecular activity within the arterial wall, consistent with plaque inflammatory activity in a Göttingen Minipig model of atherosclerosis. The data allow for future guidance in use of ^{18}F-FDG-PET/MRI both in terms of understanding disease processes in pre-clinical models and their translatability but also in drug development, providing better support for clinical development studies.

Conflicts of interest

TPL, AV, RKK, BØC are all full time employees at Novo Nordisk A/S. HDP is full time employee at Ellegaard Göttingen Minipigs A/S.

Author contributions

TPL: Conceived the study, designed and performed the experiment, handled *ex vivo* tissue, data analysis and wrote the manuscript.

SFP: Conceived the study, designed and performed the experiment, handled *ex vivo* tissue and wrote the manuscript.

RSR, HHJ, AEH, JL, TLK: Designed the imaging protocols, wrote the manuscript.

AV: Designed and performed the experiment, wrote the manuscript.

CSP: Performed the experiment, wrote the manuscript.

RKK, MØJ: Handled *ex vivo* tissue, wrote the manuscript.

HDP, BØC, LHO: Conceived the study, designed the experiment, wrote the manuscript.

JLF: Analyzed data, wrote the manuscript.

AK: Conceived the study, designed the experiment, designed imaging protocols, wrote the manuscript.

Financial support

Novo Nordisk A/S financed the experimental part of the study as well as a postdoc fellowship for TPL. The *in vivo* imaging part of the experiment was generously supported by the European Research Council (ERC) under the European Union's Horizon 2020 research and innovation programme (grant agreement No 670261), the H2020 programme, the Lundbeck Foundation, the Novo Nordisk Foundation, the Innovation Fund Denmark, the Danish Cancer Society, Arvid Nilsson Foundation, Svend Andersen Foundation, the Neye Foundation, the Research Foundation of Rigshospitalet, the Danish National Research Foundation (grant 126), the Research Council of the Capital Region of Denmark, the John and Birthe Meyer Foundation and Research Council for Independent Research.

Acknowledgements

Marianne Federspiel, Jakup Martin Poulsen, Karin Stahr (Rigshospitalet), Anders Hagedal Uhrenfeldt, Ann-Christin Løff and Pernille Kristiane Pedersen, Susanne Juhl Rasmussen, Charity M.K. Graae and Bettina Brandrup (Novo Nordisk A/S) and Henriette Vorsholdt, Danish Technical University are gratefully acknowledged for technical support and Dr. Camilla Ingvorsen, Novo Nordisk A/S for support in image analysis in histology and Dr. Peter P.M.Heegaard for ELISA analyses of C-reactive protein.

Appendix A. Supplementary data

Supplementary data to this article can be found online at https://doi.org/10.1016/j.atherosclerosis.2019.04.209.

References

[1] E.J. Benjamin, M.J. Blaha, S.E. Chiuve, et al., Heart disease and stroke statistics-2017 update: a report from the American heart association, Circulation 135 (2017) e146–e603.
[2] J.F. Bentzon, F. Otsuka, R. Virmani, E. Falk, Mechanisms of plaque formation and rupture, Circ. Res. 114 (2014) 1852–1866.
[3] M.R. Dweck, E. Aikawa, D.E. Newby, et al., Noninvasive molecular imaging of disease activity in atherosclerosis, Circ. Res. 119 (2016) 330–340.
[4] J.M. Tarkin, F.R. Joshi, J.H. Rudd, PET imaging of inflammation in atherosclerosis, Nat. Rev. Cardiol. 11 (2014) 443–457.
[5] A.L. Figueroa, A. Abdelbaky, Q.A. Truong, et al., Measurement of arterial activity on routine FDG PET/CT images improves prediction of risk of future CV events, JACC Cardiovasc Imaging 6 (2013) 1250–1259.
[6] Y-x Ye, C. Calcagno, T. Binderup, et al., Imaging macrophage and hematopoietic progenitor proliferation in atherosclerosis, Circ. Res. 117 (10) (2015) 835–845.
[7] E.J. Folco, Y. Sheikine, V.Z. Rocha, et al., Hypoxia but not inflammation augments glucose uptake in human macrophages: implications for imaging atherosclerosis with 18fluorine-labeled 2-deoxy-D-glucose positron emission tomography, J. Am. Coll. Cardiol. 58 (2011) 603–614.
[8] S.F. Pedersen, M. Graebe, A.M. Fisker Hag, L. Højgaard, H. Sillesen, A. Kjaer, Gene expression and ^{18}FDG uptake in atherosclerotic carotid plaques, Nucl. Med. Commun. 31 (2010) 423–429.
[9] N. Pipitone, C. Salvarani, A. Versari, Do we need FDG-PET/CT to assess atherosclerosis? Eur. J. Nucl. Med. Mol. Imaging 44 (2016) 247–248.
[10] A. Tawakol, Z.A. Fayad, R. Mogg, et al., Intensification of statin therapy results in a rapid reduction in atherosclerotic inflammation: results of a multicenter fluorodeoxyglucose-positron emission tomography/computed tomography feasibility study, J. Am. Coll. Cardiol. 62 (2013) 909–917.
[11] H. Emami, E. Vucic, S. Subramanian, et al., The effect of BMS-582949, a P38 mitogen-activated protein kinase (P38 MAPK) inhibitor on arterial inflammation: a multicenter FDG-PET trial, Atherosclerosis 240 (2015) 490–496.
[12] P. Libby, Murine "model" monotheism: an iconoclast at the altar of mouse, Circ. Res. 117 (2015) 921–925.
[13] P. Libby, Assisted living in the atheroma: elderly macrophages promote plaques, Cell Metabol. 24 (2016) 779–781.
[14] J.F. Bentzon, E. Falk, Atherosclerotic lesions in mouse and man: is it the same disease? Curr. Opin. Lipidol. 21 (2010) 434–440.
[15] A. Agarwala, J. Billheimer, D.J. Rader, Mighty minipig in fight against cardiovascular disease, Sci. Transl. Med. 5 (2013) 166fs1-fs1.
[16] T.P. Ludvigsen, R.K. Kirk, B.O. Christoffersen, et al., Gottingen minipig model of diet-induced atherosclerosis: influence of mild streptozotocin-induced diabetes on lesion severity and markers of inflammation evaluated in obese, obese and diabetic, and lean control animals, J. Transl. Med. 13 (2015) 312.
[17] J. Shim, R.H. Al-Mashhadi, C.B. Sørensen, J.F. Bentzon, Large animal models of atherosclerosis – new tools for persistent problems in cardiovascular medicine, J. Pathol. 238 (2016) 257–266.
[18] L.J. Andreasen, S. Krog, T.P. Ludvigsen, et al., Dietary normalization from a fat, fructose and cholesterol-rich diet to chow limits the amount of myocardial collagen in a Göttingen Minipig model of obesity, Nutr. Metab. 15 (2018) 64.
[19] C. Schumacher-Petersen, B.Ø. Christoffersen, R.K. Kirk, T.P. Ludvigsen, N.E. Zois, H.D. Pedersen, M. Vyberg, L.H. Olsen, Experimental non-alcoholic steatohepatitis in Göttingen Minipigs: consequences of high fat-fructose-cholesterol diet and diabetes, J Transl Med 17 (1) (2019 Apr 3) 110, https://doi.org/10.1186/s12967-019-1854-y PMID: 30943987.
[20] P.M. Heegaard, H.G. Pedersen, A.L. Jensen, U. Boas, A robust quantitative solid phase immunoassay for the acute phase protein C-reactive protein (CRP) based on cytidine 5'-diphosphocholine coupled dendrimers, J. Immunol. Methods 343 (2009) 112–118.
[21] S.F. Pedersen, T.P. Ludvigsen, H.H. Johannesen, et al., Feasibility of simultaneous PET/MR in diet-induced atherosclerotic minipig: a pilot study for translational imaging, Am J Nucl Med Mol Imaging 4 (2014) 448–458.
[22] J.H.F. Rudd, E.A. Warburton, T.D. Fryer, et al., Imaging atherosclerotic plaque inflammation with [^{18}F]-Fluorodeoxyglucose positron emission tomography, Circulation 105 (2002) 2708–2711.
[23] A. Martinez-Moller, M. Souvatzoglou, G. Delso, et al., Tissue classification as a potential approach for attenuation correction in whole-body PET/MRI: evaluation with PET/CT data, J. Nucl. Med. 50 (2009) 520–526.
[24] R. Virmani, F.D. Kolodgie, A.P. Burke, A. Farb, S.M. Schwartz, Lessons from sudden coronary death: a comprehensive morphological classification scheme for atherosclerotic lesions, Arterioscler. Thromb. Vasc. Biol. 20 (2000) 1262–1275.
[25] R.H. Al-Mashhadi, C.B. Sorensen, P.M. Kragh, et al., Familial hypercholesterolemia and atherosclerosis in cloned minipigs created by DNA transposition of a human PCSK9 gain-of-function mutant, Sci. Transl. Med. 5 (2013) 166ra1.
[26] S.F. Pedersen, M. Graebe, A.M. Hag, L. Hoejgaard, H. Sillesen, A. Kjaer, Microvessel density but not neoangiogenesis is associated with 18F-FDG uptake in human atherosclerotic carotid plaques, Mol. Imag. Biol. 14 (2012) 384–392.
[27] S.F. Pedersen, M. Græbe, A.M.F. Hag, L. Højgaard, H. Sillesen, A. Kjær, (18)F-FDG imaging of human atherosclerotic carotid plaques reflects gene expression of the key hypoxia marker HIF-1α, Am J Nucl Med Mol Imaging 3 (2013) 384–392.
[28] K. Skovgaard, S. Mortensen, M. Boye, et al., Rapid and widely disseminated acute phase protein response after experimental bacterial infection of pigs, Vet. Res. 40 (2009) 23.
[29] R Core Team, R: A Language and Environment for Statistical Computing, R Foundation for Statistical Computing, Vienna, Austria, 2017 URL http://www.R-project.org/.
[30] A.S. Daoud, J. Jarmolych, J.M. Augustyn, K.E. Fritz, Sequential morphologic studies of regression of advanced atherosclerosis, Arch. Pathol. Lab Med. 105 (1981) 233–239.
[31] D.N. Kim, J. Schmee, H.T. Ho, W.A. Thomas, The "turning off" of excessive cell replicative activity in advanced atherosclerotic lesions of swine by a regression diet, Atherosclerosis 71 (1988) 131–142.
[32] J. Bucerius, F. Hyafil, H.J. Verberne, et al., Position paper of the cardiovascular committee of the european association of nuclear medicine (EANM) on PET imaging of atherosclerosis, Eur. J. Nucl. Med. Mol. Imaging 43 (2016) 780–792.
[33] A. Tawakol, P. Singh, J.H.F. Rudd, et al., Effect of treatment for 12 Weeks with rilapladib, a lipoprotein-associated phospholipase A2 inhibitor, on arterial inflammation as assessed with 18F-Fluorodeoxyglucose-Positron emission tomography imaging, J. Am. Coll. Cardiol. 63 (2014) 86–88.
[34] L.J. Menezes, C.W. Kotze, O. Agu, et al., Investigating vulnerable atheroma using combined (18)F-FDG PET/CT angiography of carotid plaque with immunohistochemical validation, J. Nucl. Med. 52 (2011) 1698–1703.

[35] S. Allahverdian, A.C. Chehroudi, B.M. McManus, T. Abraham, G.A. Francis, Contribution of intimal smooth muscle cells to cholesterol accumulation and macrophage-like cells in human atherosclerosis, Circulation 129 (2014) 1551–1559.
[36] A. Tawakol, R.Q. Migrino, G.G. Bashian, et al., In vivo 18F-fluorodeoxyglucose positron emission tomography imaging provides a noninvasive measure of carotid plaque inflammation in patients, J. Am. Coll. Cardiol. 48 (2006) 1818–1824.
[37] A.V. Finn, M. Nakano, R. Polavarapu, et al., Hemoglobin directs macrophage differentiation and prevents foam cell formation in human atherosclerotic plaques, J. Am. Coll. Cardiol. 59 (2012) 166–177.
[38] L. Guo, H. Akahori, E. Harari, et al., CD163+ macrophages promote angiogenesis and vascular permeability accompanied by inflammation in atherosclerosis, J Clin Investn 128 (2018) 1106–1124.
[39] M. Aikawa, E. Rabkin, Y. Okada, et al., Lipid lowering by diet reduces matrix metalloproteinase activity and increases collagen content of rabbit atheroma: a potential mechanism of lesion stabilization, Circulation 97 (1998) 2433–2444.
[40] X.D. Xia, Z. Zhou, X.H. Yu, X.L. Zheng, C.K. Tang, Myocardin: a novel player in atherosclerosis, Atherosclerosis 257 (2017) 266–278.
[41] I. Tabas, G. Garcia-Cardena, G.K. Owens, Recent insights into the cellular biology of atherosclerosis, J. Cell Biol. 209 (2015) 13–22.
[42] C.V. Bourantas, H.M. Garcia-Garcia, V. Farooq, et al., Clinical and angiographic characteristics of patients likely to have vulnerable plaques: analysis from the PROSPECT study, JACC Cardiovasc Imaging 6 (2013) 1263–1272.
[43] Y. Zhang, E. Guallar, Y. Qiao, B.A. Wasserman, Is carotid intima-media thickness as predictive as other noninvasive techniques for the detection of coronary artery disease? Arterioscler. Thromb. Vasc. Biol. 34 (2014) 1341–1345.
[44] E. Marsch, J.C. Sluimer, M.J. Daemen, Hypoxia in atherosclerosis and inflammation, Curr. Opin. Lipidol. 24 (2013) 393–400.
[45] N.V. Joshi, I. Toor, A.S. Shah, et al., Systemic atherosclerotic inflammation following acute myocardial infarction: myocardial infarction begets myocardial infarction, J Am Heart Assoc 4 (2015) e001956.
[46] R.H. Al-Mashhadi, M.M. Bjorklund, M.B. Mortensen, et al., Diabetes with poor glycaemic control does not promote atherosclerosis in genetically modified hypercholesterolaemic minipigs, Diabetologia 58 (2015) 1926–1936.
[47] R.S. Fenning, M.E. Burgert, D. Hamamdzic, et al., Atherosclerotic plaque inflammation varies between vascular sites and correlates with response to inhibition of lipoprotein-associated phospholipase A2, J Am Heart Assoc 4 (2015) 2.
[48] S. Dalager, W.P. Paaske, I.B. Kristensen, J.M. Laurberg, E. Falk, Artery-related differences in atherosclerosis expression: implications for atherogenesis and dynamics in intima-media thickness, Stroke 38 (2007) 2698–2705.
[49] J.H. Rudd, K.S. Myers, S. Bansilal, et al., Relationships among regional arterial inflammation, calcification, risk factors, and biomarkers: a prospective fluorodeoxyglucose positron-emission tomography/computed tomography imaging study, Circ Cardiovasc Imaging 2 (2009) 107–115.
[50] E.K. Oikonomou, M. Marwan, M.Y. Desai, et al., Non-invasive detection of coronary inflammation using computed tomography and prediction of residual cardiovascular risk (the CRISP CT study): a post-hoc analysis of prospective outcome data, Lancet 392 (2018) 929–939.